Interactions between DNA and the Hfq Amyloid-like Region Trigger a Viscoelastic Response

Omar El Hamoui, Indresh Yadav, Milad Radiom, Frank Wien, Jean-Francois Berret, Johan R. C. van der Maarel, and Véronique Arluison*

Cite This: https://dx.doi.org/10.1021/acs.biomac.0c00747
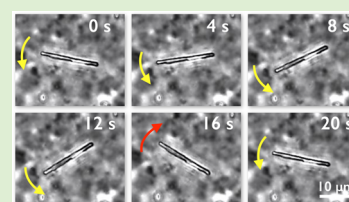
Read Online

ACCESS | Metrics & More | Article Recommendations | Supporting Information

ABSTRACT: Molecular transport of biomolecules plays a pivotal role in the machinery of life. Yet, this role is poorly understood due the lack of quantitative information. Here, the role and properties of the C-terminal region of *Escherichia coli* Hfq is reported, involved in controlling the flow of a DNA solution. A combination of experimental methodologies has been used to probe the interaction of Hfq with DNA and to measure the rheological properties of the complex. A physical gel with a temperature reversible elasticity modulus is formed due to the formation of noncovalent cross-links. The mechanical response of the complexes shows that they are inhomogeneous soft solids. Our experiments indicate that the Hfq C-terminal region could contribute to the genome's mechanical response. The reported viscoelasticity of the DNA-protein complex might have implications for cellular processes involving molecular transport of DNA or segments thereof.

INTRODUCTION

Cells are highly complex superstructures, made of different subcellular structures surrounded by one or two membranes (i.e., for Gram-negative bacteria). Eukaryotic cells, for instance, contain organelles, such as mitochondria, golgi apparatus, and nucleus. The nucleus is the largest organelle that encloses genetic information. Nucleus content is separated from the cytoplasm by the nuclear membrane, inside which the DNA is shaped by proteins to form the compacted chromatin. DNA is transcribed into RNA in the nucleus, exported to the cytoplasm through nuclear pores, and eventually translated into proteins. Bacteria lack a membrane-surrounded nucleus, and DNA, RNA, and proteins are not separated in the cytoplasm. The advantage of this arrangement is that it has a direct consequence on the speed of the transfer of genetic information. Moreover, the processes of replication, transcription, and translation all occur within the same cellular compartment. However, despite the absence of intracellular membranes, bacteria have an intracellular spatial organization.[1] For instance, they have a bacterial cytoskeleton responsible for cell division[2] or nanostructures dedicated to RNA metabolism.[3] One of the most complex structures of the bacterial cell is probably its genome, a circular chromosomic DNA. The bacterial genome is highly compacted and forms a structure called nucleoid.[4] In terms of dimensions, it is estimated that the 1 mm long bacterial genomic DNA is compacted to a nucleoid volume of $\sim$0.15 μm^3.[5] Random coil chromosomal DNA would occupy a volume of $\sim$500 μm^3.[4] Several factors affect DNA compaction and the formation of the nucleoid, including: (i) molecular crowding involving DNA segregation through overall repulsion between the components of the system;[6,7] (ii) supercoiling of genomic DNA (in *Escherichia*

coli, DNA is negatively supercoiled);[6,8] (iii) RNA stabilization;[4,9] (iv) short and long-range interactions mediated by proteins.[10] The action of different proteins, including nucleoid-associated proteins (NAPs) strongly influence DNA compaction.[10] In *E. coli*, NAPs are abundant and represent 50 000 to 200 000 proteins per cell.[11] They are known to bend or bridge DNA and/or to form filaments on DNA.[10,12,13] The resulting effect of NAPs is that the nucleoid is composed of topologically dynamic domains forming toroids, filaments, or plectonemes.[14] Thus, the nucleoid is far from being randomly organized; it is fairly structured and includes linear ordering and local alignments.[15,16] This structuring induces DNA mechanical tensions that are connected to genetic regulation and affects certain regulatory processes.[17-20]

Indeed, to function properly, sigma factors and polymerases, among other proteins, must diffuse through this densely packed DNA to find their binding sites. For this reason, too much supercoiling and constraints are harmful to the cell as they may block transcription, replication, or chromosome segregation. Proteins involved in these processes find specific sites on DNA by a combination of one-dimensional (1D) diffusion along the DNA molecule and three-dimensional (3D) diffusion through the immersion medium from a particular binding site to another site (hopping and jumping).[18,21] The resulting diffusion constant of a protein in a bacterium such as

E. coli is usually about 0.4 $\mu m^2/s$ with the highest mobility in the nucleoid region.[22,23] Protein diffusion depends on the crowding, degree of confinement, and spatial organization of the genome.[6,7] Here, we show for the first time that a part of a bridging-protein (i.e., the C-terminal region of Hfq) directly changes the DNA's viscoelasticity. We surmise that this result provides a new role for NAPs on target search because protein diffusion involves hydrodynamic interactions and flow of the genome by, among others, moving DNA segments out of the way.[4]

Our analysis focuses on an NAP called Hfq, found in about half of the bacterial species.[24] Since its identification in RNA bacteriophage Qβ replication (which gives its name host factor for bacteriophage Qβ[25]), many functions have been identified for Hfq, mainly related to RNA metabolism.[26] Indeed, Hfq exhibits a pleiotropic role, covering a wide range of functions in bacterial survival.[27] These include resistance to various stresses, influence on the growth rate, pathogenesis, mutagenesis rate, and in plasmid compaction and supercoiling.[26−31] Most of these phenotypes could be explained by the involvement of Hfq in small noncoding RNA (sRNA)-based regulation. Hfq promotes the pairing of sRNAs to their target mRNAs, mediating posttranscriptional regulation (mRNA stability and translation efficiency).[32,33] But in addition, Hfq also interacts with DNA and plays a role in bacterial DNA compaction, although its distribution within the nucleoid might be more heterogeneous than the most common NAPs, H-NS, and HU.[31,34] Therefore, while the overall minimal concentration of nucleoid Hfq is about 10−15 μM,[35,36] its concentration must vary locally from tens to hundreds of μM, with important consequences on DNA compaction and alignment.[16,30] Some of the phenotypes of hfq mutant cells, such as changes in growth rate and mutation sensitivity, may be related to its DNA-binding properties.

Structurally, Hfq is related to the Sm protein family that is also involved in RNA-related processes such as splicing and RNA degradation.[37] Hfq forms a toroidal ring similar to Sm proteins, except that in bacteria the torus consists of homohexameric oligomers, whereas in archaea and eukaryotes it tends to be formed by homo or heteroheptameric oligomers. The amino-terminal region of Hfq (NTR, about 65 aminoacid residues) is formed by an antiparallel β-sheet followed by an N-terminal α-helix; the NTR bent β-sheets of each monomer interact to form the hexameric torus. Both faces (called proximal and distal faces) and the rim of the toroidal hexamer can come into contact with the nucleic acid, but DNA is rather bound to the proximal face, i.e., the surface with the N-terminal α-helices.[38,39] On the other hand, the C-terminal region (CTR) of Hfq comprises about 40 amino acid residues outside of the Sm NTR ring, although no 3D structure is known for this CTR. Nevertheless, the CTR also binds DNA and it has been shown that it self-assembles into an amyloid-like structure in vitro and in vivo.[40,41] Recently, this CTR region has been shown to play a major role in DNA bridging and compaction[30,31] but does not directly affect the overall DNA topology.[30] In this work, we investigate a new property of the amyloid-like region of Hfq, specifically its ability to change the properties of the flow of DNA. We have opted to investigate the CTR rather than full-length Hfq, thereby avoiding complications related to changes in the secondary structure and partial melting of double-stranded DNA.[42,43] Plausible functional consequences on gene expression will also be discussed.

■ EXPERIMENTAL SECTION

Hfq C-Terminal (CTR) Peptide Synthesis and Preparation. The peptide corresponding to the amyloid CTR domain of Hfq (residues 64−102, referred to as Hfq-CTR throughout the article) was synthesized by Proteogenix SA (France). The sequence of the Hfq-CTR peptide is SRPVSHHSNNAGGGTSSNYHHGSSAQNT-SAQQDSEETE. Hfq-CTR was reconstituted in water at 20 mg/mL. The self-assembly into large fibers is not instantaneous, and the time needed to observe aggregation is dependent on the temperature and the presence of DNA[30] (in full-length Hfq, the CTR of individual subunits are attached to the torus and such a high concentration or time may not be necessary). As a negative control, a mutant peptide unable to bind DNA and consequently self-assemble (see below) within the experimental timeframe was also analyzed. Its sequence is SRPVSHHSNNAGGGT<u>AA</u>NYHHGSSAQNTSAQQDSEETE (Hfq-CTRS80,81A).

Preparation of the Complexes for SRCD and Microrheology. Complexes between Hfq-CTR peptides and the $(dA:dT)_{59}$ DNA duplex (Eurogentec) were prepared, as previously described.[16,30] We chose this $(dA:dT)_{59}$ DNA sequence because CTR has the best affinity for AT-rich sequences (∼250 nM[43]). It is important to avoid using longer DNAs as they may partially align naturally without Hfq-CTR.[16,44] In our experiments, the DNA:CTR stoichiometry varies and is always expressed in Hfq-CTR peptide and base pair (bp) concentrations (Table 1). Samples were analyzed at specific times, usually after about 2 weeks to allow peptide self-assembly on DNA that might not be instantaneous.[30]

Table 1. List of DNA/CTR Samples Studied and Experimental Conditions Used

DNA $(dA:dT)_{59}$ (mM in bp)	CTR (mM)	DNA:CTR stoichiometry	technique	apparent rheological behavior
7.3	0	1:0	wire, bead	viscous liquid
1.8	1.8	1:1	bead	gel
7.8	3.9	2:1	bead	gel
7.3	1.8	4:1	wire, bead, SRCD	gel
0	1.8	0:1	wire	viscous liquid

Wire-Based Microrheology. The magnetic wire microrheology (μ-rheology) technique has been described previously.[45−47] In brief, wires were synthesized by electrostatic co-assembly of iron oxide nanoparticles (NPs) and with poly(diallyldimethylammonium chloride) (PDADMAC, Aldrich, M_w > 100 000 g mol^{-1}).[48] NPs of sizes 6.7 and 13.2 nm were used for the synthesis, resulting in wires with different magnetization properties. Low viscosity fluids such as DNA and CTR solutions were studied with wires made with the smaller NPs, whereas experiments of the DNA-CTR gels were conducted with wires made from the larger ones. The geometrical characterization of the wires was performed by measuring the length (L) and the diameter (D) of >100 wires using a 100× objective on an optical microscope (Olympus IX73) coupled with a CCD camera (QImaging, EXi Blue) supported by software Metaview (Universal Imaging). From the distribution, we determined the reduced wire length, $L^* = L/[D\sqrt{g(L/D)}]$, where $g(x) = \ln(x) - 0.662 + 0.917/x - 0.050/x^2$.[45,49] The magnetic wires used in this study have lengths between 10 and 100 μm and diameters between 0.6 and 2 μm. We observed that the wire diameter slightly increases with L, probably due to bundle formation. As a result, scaling laws of the form $L^*(L) = \alpha L^{\beta}$ were found with $(\alpha, \beta) = 1.92$ and 0.615 for the 6.7 nm NPs and $(\alpha, \beta) = 1.66$ and 0.638 for the 13.2 nm NPs. A volume of 0.5 μL containing 10^5 wires in phosphate buffered saline (PBS, pH 7.4) was then added to the DNA, CTR, or DNA-CTR dispersions and gently stirred. A volume equal to 25 μL of this dispersion was then deposited on a glass plate and sealed into a Gene Frame (Abgene/Advanced Biotech, dimensions 10 × 10 × 0.25 mm^3). The glass plate was

introduced into a homemade device generating a rotational magnetic field, from two pairs of coils (resistance 23 Ω) working with a 90°-phase shift. An electronic setup allowed measurements in the frequency range $\omega = 10^{-2}-10^{2}$ rad s^{-1} and at a magnetic field $\mu_0 H = 10.3$ mT. The μ-rheology protocol used is based on the Magnetic Rotational Spectroscopy technique.[46,50,51] For each condition of the magnetic field and angular frequency, a movie was recorded for a period of time of at least $10/\omega$ and then treated using ImageJ software. For calibration, experiments were performed in water–glycerol solutions of viscosities between 5 and 100 mPa s at room temperature, leading to a susceptibility anisotropy coefficient $\Delta\chi = 0.054 \pm 0.006$ for the 6.7 nm NPs and $\Delta\chi = 2.3 \pm 0.5$ for the 13.2 nm NPs.[52,53]

Passive Microrheology (Particle Video Tracking). Particle tracking experiments were carried out with a Nikon Eclipse Ti-U microscope equipped with a 100× long working distance objective. The temperature was controlled with a Linkam heating stage. The samples were spiked with polystyrene microspheres (Polysciences, Warrington, PA) of 1.93 ± 0.05 μm diameter with a final concentration of 0.005 wt %. A sample having a volume of 10 μL was deposited on a microscope slide and sealed with a cover slip separated by a spacer of thickness 0.12 mm and a cavity diameter of 1 cm. To minimize hydrodynamic interactions, the selected beads for imaging were separated by at least 10 bead diameters (20 μm). Furthermore, the height level of the focal plane was adjusted so that it is situated right between the slide and cover slip with maximum separation. The trajectories of 10−25 different beads in randomly chosen locations were recorded with a complementary metal-oxide-semiconductor (CMOS) camera (Basler A504 k) at a rate of 250 frames per second. Video clips of 5 min duration were analyzed with MATLAB (Natick, MA) and the particle trajectories were obtained with public domain tracking software (http://site.physics.georgetown.edu/matlab/). All further data analysis was done with home-developed software scripts written in MATLAB code. A pixel resolution of 0.12 μm was calibrated with the help of a metric ruler. We have checked our setup by monitoring immobilized beads adsorbed to the glass slide. These beads exhibited a mean square displacement of 10^{-5} μm^2, which sets a limit to the lowest measurable creep compliance J of 0.02 m^2/N.

Electrophoretic Mobility Shift Assay (EMSA). The binding of Hfq-CTRs to DNA was investigated with EMSA. The DNA fragment was incubated with Hfq-CTR (WT and mutant) at room temperature for 20 min. EMSAs were carried out using a nondenaturing gradient 4−12% polyacrylamide gel (Bio-rad). The native gel was run for 2 h at room temperature with 40 mM Tris-acetate, 1 mM ethylenediaminetetraacetic acid, pH 8.0 (TAE) buffer, stained with the GelRed nucleic acid stain (Biotium), and imaged with a G-BOX system (Syngene, Cambridge, U.K.).

Synchrotron Radiation Circular Dichroism (SRCD). For SRCD analysis, measurements and data collection were carried out on the DISCO beamline at the SOLEIL synchrotron (proposal 20171061).[54] Two to four microliters of samples were loaded into circular demountable CaF$_2$ cells of 33 μm pathlength.[55] Three separate data collections with fresh sample preparations were carried out to ensure consistency and repeatability. Spectral acquisitions of 1 nm steps at 1.2 s integration time, between 320 and 180 nm were performed in triplicate for the samples as well as for the baselines. (+)-camphor-10-sulfonic acid (CSA) was used to calibrate amplitudes and wavelength positions of the SRCD experiment. Data analyses including averaging, baseline subtraction, smoothing, scaling, and standardization were carried out with CDtool.[56]

■ RESULTS AND DISCUSSION

Binding of Hfq-CTR to DNA. We first confirmed the interaction of the Hfq-CTR peptide and our model (dA:dT)$_{59}$ DNA with electrophoretic mobility shift assay (EMSA) and synchrotron radiation circular dichroism (SRCD). The EMSA result is shown in Figure 1A. A clear band shift is observed in the case of the wild type (WT) Hfq-CTR, confirming strong
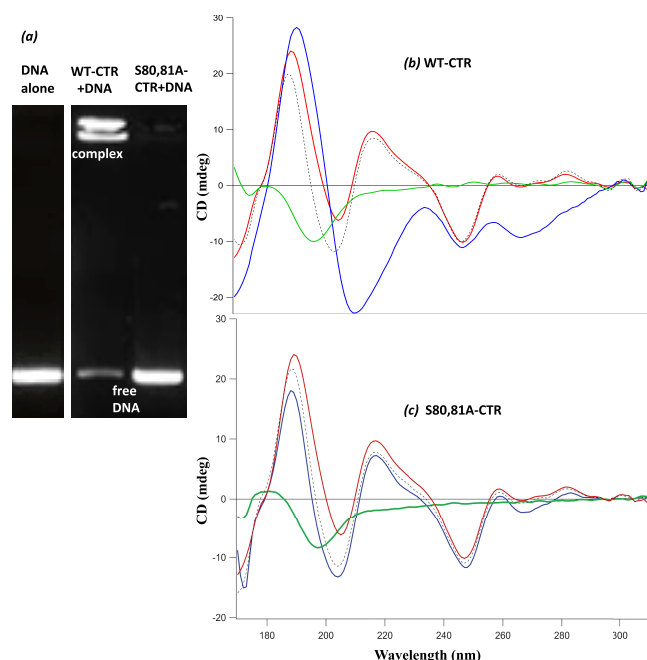

Figure 1. (a) EMSA analysis of Hfq-CTR wild type (WT-CTR) and the mutant (S80,81A-CTR) in the presence of DNA. DNA alone; DNA in the presence of WT-CTR; DNA in the presence of the S80,81A-CTR mutant. EMSA shows that the mutant does not bind to DNA, while WT-CTR does. Note that 2 complexes of different sizes are formed by the WT Hfq-CTR, probably due to different numbers of CTRs bound to DNA. (b) SRCD spectra of the WT-CTR/DNA complex (blue), DNA (red), and WT-CTR (green). The dotted spectrum represents the relevant combination of the spectra pertaining to the individual components. (c) As in panel (b) but for S80,81A-CTR.

binding.[16,30] No band shift is observed upon addition of the Hfq-CTRS80,81A mutant. This indicates that the CTR mutant does not bind DNA, at least to a degree which can be detected with the EMSA assay. Binding by WT Hfq-CTR and the absence of binding by the Hfq-CTRS80,81A mutant to DNA were confirmed with SRCD. The spectra pertaining to WT-CTR and mutant S80,81A-CTR are shown in Figure 1B,C, respectively. Spectra of the individual components as measured from solutions with equivalent DNA and CTR concentrations are also displayed. For WT-CTR, significant spectral changes in the 220 nm region (inversion of CD signal) and 260−280 nm spectral band are observed. These correlate with previously identified amyloid formation, base tilting, and base pairing of AT-rich sequences, respectively.[16] Furthermore, the relevant combination of the spectra pertaining to the individual components does not match the spectrum of the WT-CTR/DNA mixture, the theoretical summation of the individual spectra does not result in the experimentally measured spectra of the complexed CTR-DNA. The observed spectral changes for WT-CTR have been associated with amyloid formation.[16,30] In contrast, following addition of S80,81A-CTR to DNA no significant differences in the SRCD spectrum were observed (Figure 1C). Here, the experimentally observed spectrum is close to the recomposed spectrum obtained from the relevant combination of the individual components. Such a small difference indicates that the interaction between S80,81A-CTR and DNA must be nonexistent or very weak (see below).

Note that, in the cell, the CTRs are attached to the toroidal assembly formed by the full-length protein. Thus, they may behave differently.[57] Nevertheless, full-length Hfq and CTR-Hfq displayed similar SRCD signals (specifically an inversion between 220−240 nm indicative of base tilting, not shown), suggesting that full-length Hfq and Hfq-CTR behave similarly. In contrast, for the Hfq-CTRS80,81A mutant-DNA complex, no such spectral differences could be observed. The experimental spectrum of the mutant complexed to DNA resembled the theoretical sum of the isolated mutant Hfq-CTR and DNA spectra. The subtle difference indicates that the interaction must be nonexistent (or rather weak). This is certainly due to the fact that within the DNA-binding region of Hfq-CTR, the change of amino acid side chains from serine to alanine does not allow the formation of hydrogen-bonding involved in the binding of the CTR to DNA, which strongly reduces the affinity.[58] These results can be explained by the fact that the Hfq-CTR mutant does not change its structure, as the DNA cannot promote the polymerization (amyloid-like) of Hfq-CTR.[30] Indeed, the spectral signature at 220 nm of amyloid formation coinciding with the DNA tilting is absent for the mutant Hfq-CTR.

DNA and CTR Dispersions Studied via Wire μ-Rheology. *Generic Behaviors: Viscous Liquid Versus Viscoelastic Solid.* Figure 2a illustrates the rotation of a 33
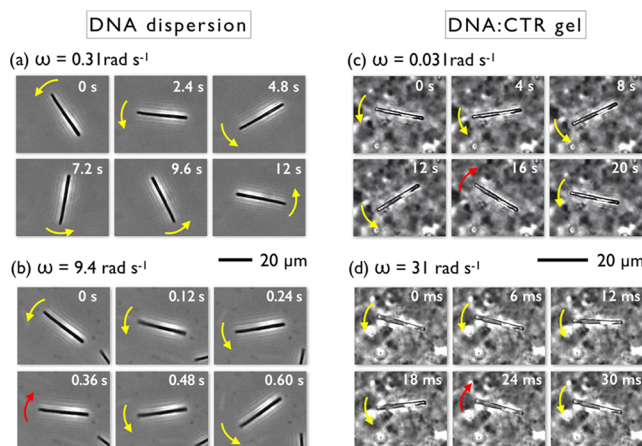

Figure 2. (a) Chronophotograph of a 33 μm (diameter 1.8 μm) wire undergoing a rotation observed in a 7.3 mM DNA dispersion under the application of a magnetic field $\mu_0 H$ = 10.3 mT and at room temperature. In this experiment, the applied actuation frequency ω is 0.31 rad s^{-1}. (b) As in (a) at ω = 9.4 rad s^{-1}. The yellow (resp. red) arrows mark the rotation in the same (resp. opposite) direction of the magnetic field. (c) Chronophotograph of a 21 μm (diameter 1.4 μm) wire undergoing an oscillatory motion in a 7.3 mM:1.8 mM DNA-CTR complex at angular frequency ω = 0.031 rad s^{-1}. (d) As in (c) at ω = 9.4 rad s^{-1}.

μm wire in a 7.3 mM (dA:dT)$_{59}$ DNA dispersion at an angular frequency ω = 0.31 rad s^{-1}, with a counter-clockwise rotation in the direction indicated by yellow arrows. The different images of the chronophotograph are taken at time intervals of 2.4 s during a 210°-rotation of the object, showing that the wire rotates synchronously with the field. By increasing the frequency to 9.4 rad s^{-1} (Figure 2b), the wire presents a transition to asynchronous rotation whereby it shows back and forth oscillations. After an initial increase in the orientation angle in the counter-clockwise direction (yellow arrows), the wire undergoes a back motion in the clockwise direction (red

arrows) followed again by an increase in the orientation angle. We refer to the transition from the synchronous to the asynchronous regime by the critical frequency ω_C. For the wire shown in Figure 2a,b, ω_C is equal to 3.7 ± 0.5 rad s^{-1}. A 1.8 mM CTR-dispersion was studied in the same conditions and revealed a similar transition with increasing ω. As reported in our work on model viscoelastic liquids and soft solids,[45,59] the previous behavior was found to be characteristic of purely viscous liquids.

For DNA-CTR complexes, similar measurements showed a notable change in the wire oscillatory behavior. Subject to the same field conditions, the wires oscillated between fixed orientations, which were independent of the angular frequency. Figure 2c,d displays chronophotographs of a 21 μm wire incorporated in a 4:1 complex and actuated at ω = 0.031 and 31 rad s^{-1}, respectively. One observes a heterogeneous background under phase contrast microscopy, which is associated with a nonuniform material distribution (as was shown by localized μ-rheology measured using bead technology, see below). This could come from heterogeneity in the formation of CTR-assembled structures on DNA with sizes in the visible light range. It is also noted that the sizes of the heterogeneous regions (∼1 μm) are smaller than the length of the wire. For this sample, the wire rotation is found to be asynchronous at all ω's, which implies that the wires do not follow the field completely for any applied actuation frequency. The observation on DNA-CTR is an indication that the material is a soft solid and characterized by a yield stress behavior. This outcome is also in line with results found in calcium ion cross-linked polysaccharide gels.[47] The videos associated with the wire rotations in Figure 2 are shown in Supporting Movies 1, 2, 3, and 4.

Quantitative Analysis. For data analysis, movies of rotating wires were recorded, treated following the procedure described in the Experimental Section, and transformed into an in-plane wire orientation angle $\theta(t)$ as a function of time. The obtained $\theta(t)$ dependences were then analyzed in a set of two parameters: the average rotation velocity $\Omega(\omega) = \langle d\theta(t)/dt \rangle_t$ and the back and forth oscillation amplitude $\theta_B(\omega) = \langle \theta_B(t,\omega) \rangle_t$. Figure 3a shows the normalized velocity $\Omega(\omega)/\omega_C$ as a function of the normalized frequency ω/ω_C for both DNA and CRT dispersions at 7.3 and 1.8 mM, respectively. We find that $\Omega(\omega)/\omega_C$ increased with the frequency in the synchronous regime ($\omega \leq \omega_C$) until it passed through a sharp maximum at ω_C and then fell rapidly ($\omega > \omega_C$). Moreover, one observes that the wire response agrees well with the predictions of the Newton constitutive equation, given by

$$\Omega(X) = X \text{ for } X \leq 1 \text{ and } \Omega(X) = X - \sqrt{X^2 - 1} \text{ for } X \geq 1$$

(continuous line).[59] Figure 3b shows the oscillation amplitude angle $\theta_B(\omega)$ as a function of the reduced frequency ω/ω_C for the same 2 samples. A good superimposition of the data points is observed and is in agreement again with the Newton prediction, $\theta_B(\omega/\omega_C) \sim (\omega/\omega_C)^{-1}$ for $\omega \gg \omega_C$ (continuous line).[45,60] Note that, in the $\theta_B(\omega/\omega_C)$-representation, the continuous line in the figure is obtained without an adjustable parameter.[45] In contrast, DNA and CTR behaved as Newton fluids at the concentrations studied here, and the dispersions were characterized by a single rheological parameter, the static shear viscosity η, determined in the next section.

Figure 3c displays the average angular velocity $\Omega(\omega)$ in 4:1 DNA-CTR dispersions for wires comprised between 19 and 80 μm and actuated in the range ω = 3 × 10^{-2}−30 rad s^{-1}. Data
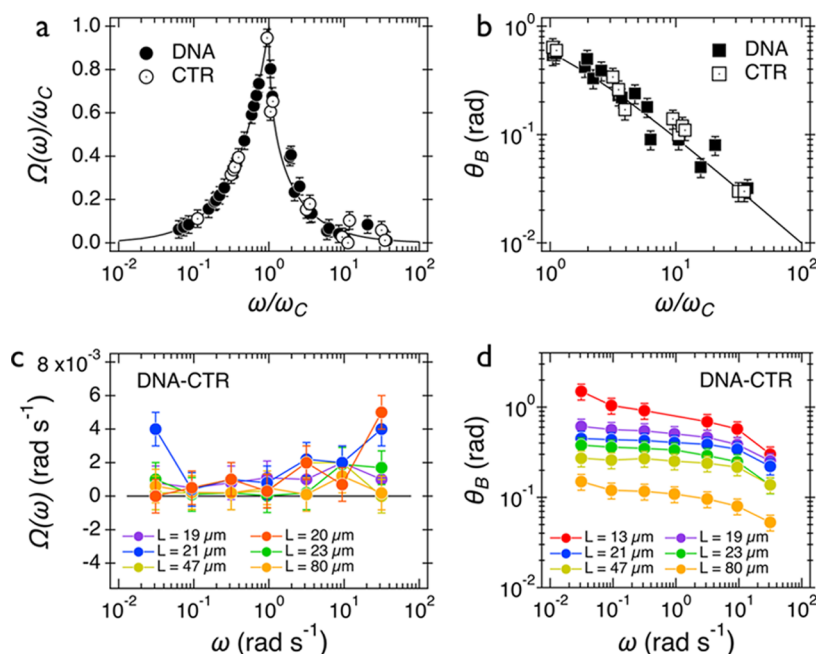
Figure 3. (a, b) Wire average rotation velocity $\Omega(\omega)$ and oscillation amplitude $\theta_B(\omega)$ measured in DNA and CTR dispersions. The continuous lines are calculated from the constitutive equations for Newton fluids. (c, d) Same as Figure 2a,b for the 4:1 DNA-CTR complex. For the mixed dispersions, $\Omega(\omega)$ is close to zero and frequency independent. The oscillation amplitude displays a strong dependency with the wire length.
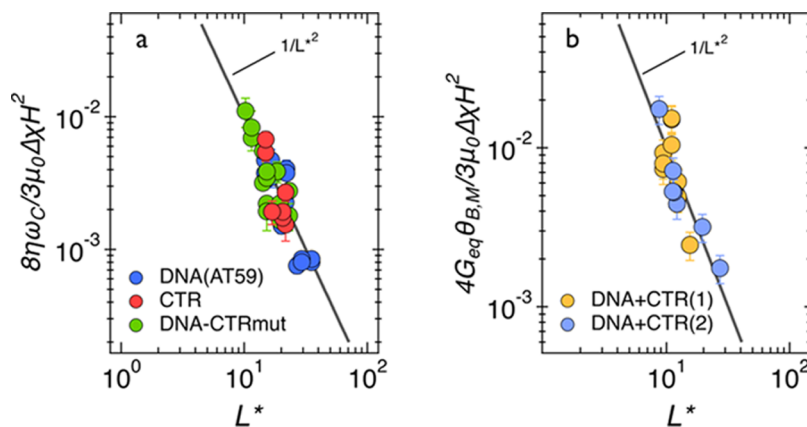

Figure 4. (a) Normalized critical frequency $8\eta\omega_C/3\mu_0\Delta\chi H^2$ as a function of the reduced wire length L^* obtained for DNA, CTR, and 4:1 DNA-Hfq-CTRS80,81A complex dispersions. The straight lines correspond to the $1/L^{*2}$ dependence predicted by the Newton constitutive equation. (b) Normalized oscillation amplitude $4G_{eq}\theta_{B,M}/3\mu_0\Delta\chi H^2$ as a function of L^* for two different samples of 4:1 DNA-CTR complexes. The straight line indicates the $1/L^{*2}$-behavior expected from the soft solid model.[47]

show that $\Omega(\omega)$ are frequency independent and close to zero. For this sample, the critical frequency ω_C cannot be found. Such behavior has been identified as resulting from soft solids, characterized by an infinite static viscosity and a yield stress. Figure 3d displays the oscillation amplitude $\theta_B(\omega)$ as a function of the frequency. $\theta_B(\omega)$ exhibits a plateau at low frequency, noted $\theta_{B,M}$, and decreases above 1 rad s^{-1}, showing again a very different behavior compared with Newton liquids (Figure 3b).

We next take advantage of the wire length dispersity and explore asymptotic behaviors, a technique that was shown to improve the accuracy in the determination of rheological parameters.[52] For $(dA:dT)_{59}$ and CTR dispersions, the viscosity can be identified from the asymptotic behavior of ω_C as a function of L^*, the reduced wire length. As shown previously,[45] ω_C is related to the static viscosity η via the expression: $\omega_C = 3\mu_0\Delta\chi H^2/8\eta L^{*2}$, where μ_0 is the vacuum

permeability, H is the magnetic field strength, and $\Delta\chi = 0.054$, the magnetic anisotropy of wires. Figure 4a displays the ratio $8\eta\omega_C/3\mu_0\Delta\chi H^2$ as a function of L^* for the DNA, CTR, and a control consisting of a complex between DNA and an Hfq-CTR mutant. This control peptide (mutant CTR) was used to show that the gelation is due specifically to the wild type Hfq-CTR properties and not to a nonspecific effect due to the presence of the protein only. This result is indicative that the Hfq-CTRS80,81A mutant is unable to bind DNA, as was discussed above (Figure 1). In Figure 4a, the data points collapse on a single master curve displaying the $1/L^{*2}$-dependence (continuous line) in agreement with the model predictions. The measured viscosities are 1.6 ± 0.3 mPa s for the DNA solution, 3.3 ± 0.8 mPa s for CTR, and 2.4 ± 0.3 mPa s for 4:1 DNA-CTRS80,81A. These values are slightly higher than the viscosity of the suspending solvent ($\eta_{PBS} = 0.90$ mPa s at 25 °C) and in line with that of a dilute solution of
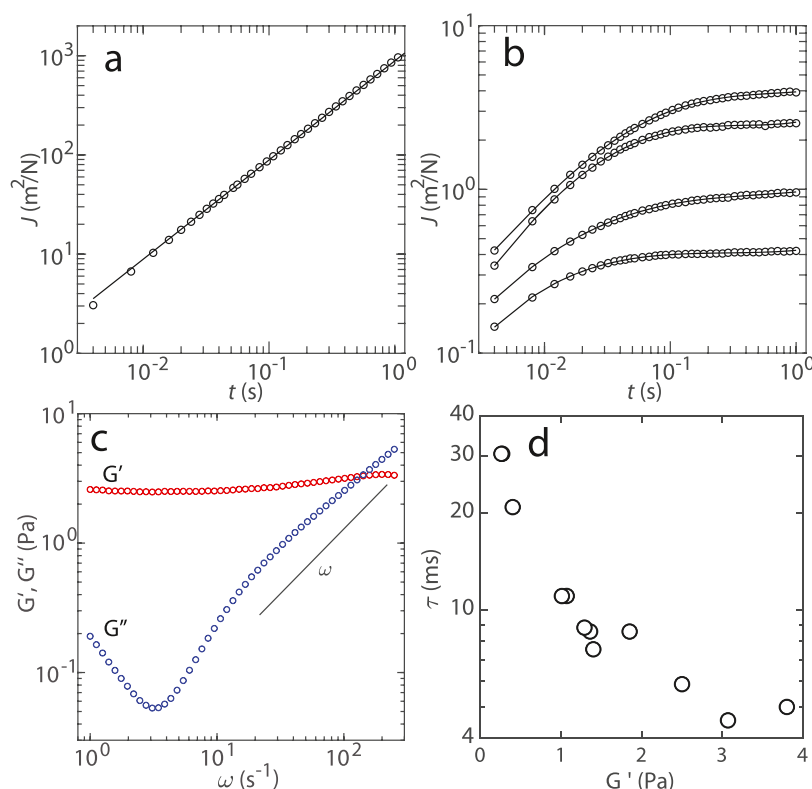
Figure 5. (a) Creep compliance J versus time t at 296 K of the model system without CTR. The DNA concentration is 1.8 mM. The solid line represents a linear fit. (b) As in panel (a) but for a 4:1 DNA-CTR dispersion at four randomly chosen bead locations inside the sample. (c) Elastic storage G' and viscous loss G' moduli versus frequency ω pertaining to the lowest creep compliance in panel (b). The solid line denotes ω scaling. (d) Low-frequency limit of G' and cross-over relaxation time $\tau = \omega_c^{-1}$ pertaining to 12 different locations.

macromolecules.[61] Given the low concentration in the CTR sample (1.8 mM), a viscosity of 3.3 mPa s may indicate possible aggregation of proteins.

From the constitutive equations developed for soft solids,[47] the low-frequency limit $\theta_{B,M}$ is linked to the equilibrium storage modulus G_{eq} through the relation $\theta_{B,M} = \lim_{\omega \to 0} \theta_B(\omega) = 3\mu_0 \Delta\chi H^2 / 4L^{*2} G_{eq}$. For a soft solid, G_{eq} characterizes the quasi-static elastic response of the material. Figure 4b shows the ratio $4G_{eq}\theta_{B,M}/3\mu_0\Delta\chi H^2$ as a function of L^* for two different samples of the DNA-CTR gel. A good superimposition of the data points is observed and agrees with the predicted $1/L^{*2}$ scaling. The equilibrium storage moduli are equal to 0.2 ± 0.03 and 1.7 ± 0.3 Pa for these two experiments, the susceptibility anisotropy coefficients being $\Delta\chi = 2.3$. The results suggest a certain variability in the modulus, which could come from fluctuations in the elasticity of the environment or from sample aging effects. In conclusion and considering the frequency range studied, the 4:1 DNA-CTR complex behaves as a soft gel with a clear viscoelastic signature, whereas a complex made with the CTR mutant is a purely viscous liquid.

DNA and CTR Dispersions Studied via Particle Tracking. *Passive Bead Microrheology of DNA and DNA-CTR Complexes.* The viscoelastic properties of the DNA-CTR dispersions were also measured with passive μ-rheology using a video tracking of colloidal beads. This method allows the measurement of the viscoelastic response in localized regions of the sample, thereby characterizing the heterogeneity in CTR-assembled structures on DNA. Furthermore, the dispersions are investigated close to the equilibrium using

low shear without causing variations in the DNA density over several microns. Formation of a physical gel can easily be recognized from plateauing bead mean square displacement for long lag times and its temperature reversible behavior.

From the trajectories of the colloidal beads, the probability distributions for displacements in the x- and y-directions were determined for a range of lag times t. Gaussians were fitted to the probability distributions by optimizing the mean square displacement $\langle \Delta x^2(t) \rangle$. The widths of the distributions obtained in the orthogonal x- and y-directions were averaged. Accordingly, $\langle \Delta x^2(t) \rangle$ refers to the mean square displacement in one dimension. We then obtained the time-dependent creep compliance according to $J(t) = 3\pi a \langle \Delta x^2(t) \rangle / k_B T$ with $k_B T$ being the thermal energy and a the radius of the bead. The results for $(dA:dT)_{59}$ and the 4:1 DNA-CTR complex obtained at ambient temperature (296 K) are shown in Figure 5a,b, respectively. Results for 1:1 and 2:1 DNA-CTR dispersions are qualitatively similar but differ in the relaxation time and elasticity modulus (see below). The creep compliance for DNA shows a viscous flow behavior according to $J(t) = t/\eta$ with static viscosity $\eta = 1.13 \pm 0.03$ mPa s. For the DNA-CTR dispersions, the temporal behavior of the creep compliance is markedly different. Here, $J(t)$ first increases and, subsequently, plateaus at a constant value ($1/G'$, see below) with increasing lag time. Furthermore, the creep compliance depends on the location of the monitored bead inside the sample (10−25 different locations were probed). We have verified that the variation in the creep compliance is not related to a variation in the bead diameter but to the inhomogeneity in the viscoelastic response.

The viscoelastic response of the DNA-CTR dispersions is more conveniently discussed in terms of the elastic storage and viscous loss moduli, G' and G'', respectively. Following the previously described procedure, we have obtained G' and G'', from the one-sided, complex Fourier transform of the creep compliance and the generalized Stokes−Einstein equation.[62] This approach requires that the fluid can be treated as an incompressible continuum, no-slip boundary conditions, and that the Stokes drag can be extended over all frequencies.[63] An example of the moduli is displayed in Figure 5c. If the bead is harmonically bound according to $\langle \Delta x^2(t) \rangle = x_o^2 [1 - \exp(-t/\tau)]$ with amplitude x_o^2 and relaxation time τ, one obtains a constant $G' = k_B T/(3\pi a x_o^2) = 1/J(t \to \infty)$, $G'' = \omega \tau G'$, and a cross-over frequency $\omega_c = \tau^{-1}$. As can be seen in Figure 5c, G' is almost constant and G'' approaches ω scaling for higher frequencies. Accordingly, the passive viscoelastic behavior of the DNA-CTR dispersions at the relevant time scale (<1 s) is close to the one of an elastic solid. As is the case for the creep compliance, G' and G'' vary across the sample. For different locations, we determined the low-frequency limit of G' and the cross-over relaxation time $\tau = \omega_c^{-1}$. The results are shown in Figure 5d (12 locations). A variation over an order of magnitude is observed with a longer relaxation time for locations with lower values of G'. Similar spatial variations over different locations were observed for the other investigated DNA-CTR dispersions. At a higher temperature, the elastic modulus decreases but the dispersions remain elastic solid-like. We have checked that the temperature-induced change in viscoelasticity is reversible. The mean values and standard deviations of G' and τ pertaining to the various investigated DNA-CTR dispersions are collected in Table 2. Note that the

Table 2. Mean Values of the Low Frequency Elasticity Modulus G', Relaxation Time τ, and Their Standard Deviations (Bracketed) at 10−25 Bead Locations across the DNA-CTR Dispersions

sample	composition	T (K)	G' (Pa)	τ (ms)
1:1 DNA-CTR	1.8 mM DNA 1.8 mM CTR	296	1.4 (0.8)	11 (5)
		303	1.1 (0.8)	13 (10)
		313	0.9 (0.7)	13 (9)
		323	0.6 (0.5)	26 (20)
		333	0.03 (0.02)	104 (60)
2:1 DNA-CTR	7.8 mM DNA 3.9 mM CTR	296	2.6 (1.0)	7 (2)
		303	1.9 (0.8)	6 (1)
		313	1.3 (0.7)	10 (4)
		323	0.7 (0.4)	11 (5)
		333	0.2 (0.1)	23 (14)
4:1 DNA-CTR	7.3 mM DNA 1.8 mM CTR	296	1.5 (1.1)	13 (9)

data were obtained by averaging results for 10−25 different locations across each sample, so that the standard deviations refer to the inhomogeneity in the viscoelastic response rather than experimental errors.

The elasticity moduli for 1:1 and 4:1 DNA-CTR complexes are similar and comparable to those which have been measured with wire rheology. An increase in the concentration of DNA but with a constant concentration of CTR has little, if any, effect on the rheological properties. On the other hand, doubling the CTR concentration at approximately the same

DNA concentration (2:1 vs 4:1 complex, Table 2) results in a gel with a higher elasticity modulus and a shorter relaxation time. These observations indicate that the compliance of the system is determined by the density of cross-links formed by complexation of CTR on DNA. An increase in temperature results in a decrease in cross-link density (cross-linking complexes are reversibly dissolved), larger but less dynamic units, and, hence, a decrease in elasticity modulus. At the subsecond time scale of the passive rheology experiment, the DNA-CTR dispersions behave close to an elastic solid. The derived relaxation times refer, hence, to thermally activated elastic deformations of the cross-linked network of DNA and CTR. For longer times, the dispersions might flow with relaxation times exceeding tens of seconds. The latter dynamics likely involves cross-link rearrangements. Unfortunately, such slow dynamics are outside the window of observation of the particle tracking experiment due to long time experimental artifacts such as drift of the microscope stage.

Finally, samples with relatively high concentrations of DNA and Hfq-CTR (6.5 mM each) exhibited separation into two coexisting phases (in agreement with the nonuniform material distribution observed previously under phase contrast microscopy, see Figure 2). One phase was a Newtonian fluid, whereas the other phase behaved as a gel. The viscoelastic response of the gel could not be measured because the beads were almost immobilized. This phase separation may help to compact the genomic DNA in vivo, as previously suggested by *in silico* analyses.[7]

■ CONCLUSIONS

The key finding of this work is that a putative DNA-binding domain of a nucleoid-associated protein assembles DNA into a gel. The interaction of DNA with the amyloid domain has been revealed by SRCD spectroscopy. The properties of the resulting gel may either be a true elastic soft solid with a yield stress value or a viscoelastic liquid with a finite viscosity. Our experiments rather suggest that it is a soft solid, the creep compliance as measured by bead tracking plateaus at a constant value for lag times of around 1 s and the lowest frequency that could be reached with the wire rheology is 0.01 rad/s. If the network has a relaxation time associated with yield to flow, it is very long (>100 s) for the range of shear stresses applied in this work. Both wire rheology with the employed range in actuation frequency and bead tracking methodology probe the linear response of the material. As shown previously, using solutions of wormlike micelles and gels made from cross-linked polysaccharides, the static viscosity determined from the wire-based rheology and that obtained from standard cone-and-plate measurements are in good agreement, indicating that actuated wires probe the linear response of the material.[45] The passive thermal motion of the embedded colloidal beads does not induce a variation in DNA density over distances exceeding their temporal displacements that is several microns. The observed inhomogeneity in elasticity modulus originates from the variation in the cross-link density, which is a characteristic property of the solution and not caused by the probing beads. In the case of wire rheology, the DNA-CTR gel deforms but does not flow or break. This is due to the fact that the stress applied by the wire is below the yield stress value of the gel. The elastic moduli obtained with both techniques agree and are around 1 Pa. Bead rheology shows, however, a variation over an order of magnitude across the sample, highlighting inhomogeneity in the density of cross-links

formed by dynamic complexation of CTR on DNA. An increase in temperature results in a reversible decrease in the cross-link density and softening of the gel.

As for in vivo consequences, our experiments suggest that a NAP not only determines the spatial organization of the genome but also properties of the flow. The latter aspect is often overlooked but should have important consequences for understanding the molecular motion of DNA and proteins in the context of the machinery of life.[6] The assembly of such DNA-protein complexes is usually rather slow, as the kinetics is limited by the diffusion of the constituents (low concentrations). Therefore, this micromechanical constraint generated by Hfq, even if it should be very local, could serve various biological processes. DNA's viscoelasticity might have implications for cellular processes, in particular those that involve transport and flow of the genome. In particular, cell division requires separation of the replicated genetic material into the daughter cells. Other examples are protein-mediated looping of chromosomal sections, chromosomal organization in topological domains,[64] and transcriptional bursting.[65−68] We surmise that the DNA's viscoelasticity also provides a new role for NAPs in protein target search because a protein diffusing through a network of DNA is affected by viscous forces (hydrodynamic interactions) and requires DNA segments moving out of the way. Another in vivo consequence of gelation might be swelling of the DNA network by an imbalance in the osmotic pressure, resulting in stress exerted on the duplex, and concomitant effects on protein binding.

■ ASSOCIATED CONTENT

ⓈSupporting Information

The Supporting Information is available free of charge at https://pubs.acs.org/doi/10.1021/acs.biomac.0c00747.

Movie#1-NW in DNA 50 mHz (AVI)
Movie#2-NW in DNA 1500 mHz (AVI)
Movie#3-NW in DNA-CTR 5 mHz (AVI)
Movie#4-NW in DNA-CTR 5000 mHz (AVI)

■ AUTHOR INFORMATION

Corresponding Author

Véronique Arluison − *Laboratoire Léon Brillouin LLB, CEA, CNRS UMR12, Université Paris Saclay, F-91191 Gif-sur-Yvette, France; Université de Paris, F-75006 Paris, France;* ⓘ orcid.org/0000-0003-4056-7282; Phone: 33 (0)1 69 08 32 82; Email: veronique.arluison@u-paris.fr

Authors

Omar El Hamoui − *Synchrotron SOLEIL, F-91192 Gif-sur-Yvette, France*

Indresh Yadav − *Department of Physics, National University of Singapore, Singapore 117542 Singapore*

Milad Radiom − *Matière et Systèmes Complexes, UMR 7057 CNRS Université de Paris, F-75205 Paris, France*

Frank Wien − *Synchrotron SOLEIL, F-91192 Gif-sur-Yvette, France;* ⓘ orcid.org/0000-0002-0752-8735

Jean-Francois Berret − *Matière et Systèmes Complexes, UMR 7057 CNRS Université de Paris, F-75205 Paris, France;* ⓘ orcid.org/0000-0001-5458-8653

Johan R. C. van der Maarel − *Department of Physics, National University of Singapore, Singapore 117542 Singapore;* ⓘ orcid.org/0000-0001-5560-0298

Complete contact information is available at:

https://pubs.acs.org/10.1021/acs.biomac.0c00747

Author Contributions

O.E.H. and I.Y. contributed equally to the work and are equal first authors. J.R.C.v.d.M., J.-F.B., F.W., and V.A. conceived the original idea and designed the experiments. O.E.H., I.Y., V.A., and F.W. performed experiments. J.R.C.v.d.M., J.-F.B., F.W., M.R., and V.A. wrote the manuscript. All authors analyzed the results and commented on the manuscript.

■ ABBREVIATIONS

bp, base pair; CTR/NTR, Hfq C/N-terminal region; EMSA, electrophoretic mobility shift assay; NAP, nucleoid-associated protein; μ-rheology, microrheology; SRCD, synchrotron radiation circular dichroism; WT, wild type

■ REFERENCES

(1) Abbondanzieri, E. A.; Meyer, A. S. More than just a phase: the search for membraneless organelles in the bacterial cytoplasm. *Curr. Genet.* **2019**, *65*, 691−694.

(2) Errington, J. Dynamic proteins and a cytoskeleton in bacteria. *Nat. Cell Biol.* **2003**, *5*, 175−178.

(3) Taghbalout, A.; Yang, Q.; Arluison, V. The *Escherichia coli* RNA processing and degradation machinery is compartmentalized within an organized cellular network. *Biochem. J.* **2014**, *458*, 11−22.

(4) Verma, S. C.; Qian, Z.; Adhya, S. L. Architecture of the *Escherichia coli* nucleoid. *PLoS Genet.* **2019**, *15*, No. e1008456.

(5) Skoko, D.; Yoo, D.; Bai, H.; Schnurr, B.; Yan, J.; McLeod, S. M.; Marko, J. F.; Johnson, R. C. Mechanism of chromosome compaction and looping by the *Escherichia coli* nucleoid protein Fis. *J. Mol. Biol.* **2006**, *364*, 777−798.

(6) Joyeux, M. Bacterial Nucleoid: Interplay of DNA Demixing andSupercoiling. *Biophys. J.* **2020**, *118*, 2141−2150.

(7) Joyeux, M. A segregative phase separation scenario of the formation of the bacterial nucleoid. *Soft Matter* **2018**, *14*, 7368−7381.

(8) de Vries, R. DNA condensation in bacteria: Interplay between macromolecular crowding and nucleoid proteins. *Biochimie* **2010**, *92*, 1715−1721.

(9) Pettijohn, D. E.; Hecht, R. RNA molecules bound to the folded bacterial genome stabilize DNA folds and segregate domains of supercoiling. *Cold Spring Harbor symp. quant. biol.* **1974**, *38*, 31−41.

(10) Dame, R. T.; Rashid, F.-Z. M.; Grainger, D. C. Chromosome organization in bacteria: mechanistic insights into genome structure and function. *Nat. Rev. Genet.* **2020**, *21*, 227−242.

(11) Xie, X. S.; Choi, P. J.; Li, G.-W.; Lee, N. K.; Lia, G. Single-molecule approach to molecular biology in living bacterial cells. *Annu. Rev. Biophys.* **2008**, *37*, 417−444.

(12) Wiggins, P. A.; Cheveralls, K. C.; Martin, J. S.; Lintner, R.; Kondev, J. Strong intranucleoid interactions organize the *Escherichia coli* chromosome into a nucleoid filament. *Proc. Natl. Acad. Sci. U.S.A.* **2010**, *107*, 4991−4995.

(13) Qin, L.; Erkelens, A. M.; Ben Bdira, F.; Dame, R. T. The architects of bacterial DNA bridges: a structurally and functionally conserved family of proteins. *Open Biol.* **2019**, *9*, No. 190223.

(14) Espeli, O.; Mercier, R.; Boccard, F. DNA dynamics vary according to macrodomain topography in the E. coli chromosome. *Mol. Microbiol.* **2008**, *68*, 1418−1427.

(15) Breier, A. M.; Cozzarelli, N. R. Linear ordering and dynamic segregation of the bacterial chromosome. *Proc. Natl. Acad. Sci. U.S.A.* **2004**, *101*, 9175−9176.

(16) Wien, F.; Martinez, D.; Le Brun, E.; Jones, N. C.; Vronning Hoffmann, S.; Waeytens, J.; Berbon, M.; Habenstein, B.; Arluison, V. The Bacterial Amyloid-Like Hfq Promotes In Vitro DNA Alignment. *Microorganisms* **2019**, *7*, 639.

(17) Milstein, J. N.; Meiners, J. C. On the role of DNA biomechanics in the regulation of gene expression. *J. R. Soc., Interface* **2011**, *8*, 1673−1681.

(18) Mondal, A.; Bhattacherjee, A. Searching target sites on DNA by proteins: Role of DNA dynamics under confinement. *Nucleic Acids Res.* **2015**, *43*, 9176−9186.

(19) Dorman, C. J.; Schumacher, M. A.; Bush, M. J.; Brennan, R. G.; Buttner, M. J. When is a transcription factor a NAP? *Curr. Opin. Microbiol.* **2020**, *55*, 26−33.

(20) Dillon, S. C.; Dorman, C. J. Bacterial nucleoid-associated proteins, nucleoid structure and gene expression. *Nat. Rev. Microbiol.* **2010**, *8*, 185−195.

(21) Chow, E.; Skolnick, J. DNA Internal Motion Likely Accelerates Protein Target Search in a Packed Nucleoid. *Biophys. J.* **2017**, *112*, 2261−2270.

(22) Elf, J.; Li, G.-W.; Xie, X. S. Probing transcription factor dynamics at the single-molecule level in a living cell. *Science* **2007**, *316*, 1191−1194.

(23) Stylianidou, S.; Kuwada, N. J.; Wiggins, P. A. Cytoplasmic dynamics reveals two modes of nucleoid-dependent mobility. *Biophys. J.* **2014**, *107*, 2684−2692.

(24) Sun, X.; Zhulin, I.; Wartell, R. M. Predicted structure and phyletic distribution of the RNA-binding protein Hfq. *Nucleic Acids Res.* **2002**, *30*, 3662−3671.

(25) Franze de Fernandez, M. T.; Hayward, W. S.; August, J. T. Bacterial proteins required for replication of phage Qβ ribonucleic acid. *J. Biol. Chem.* **1972**, *247*, 824−831.

(26) Kavita, K.; de Mets, F.; Gottesman, S. New aspects of RNA-based regulation by Hfq and its partner sRNAs. *Curr. Opin. Microbiol.* **2018**, *42*, 53−61.

(27) Tsui, H. C.; Leung, H. C.; Winkler, M. E. Characterization of broadly pleiotropic phenotypes caused by an hfq insertion mutation in *Escherichia coli* K-12. *Mol. Microbiol.* **1994**, *13*, 35−49.

(28) Chen, J.; Gottesman, S. Hfq links translation repression to stress-induced mutagenesis in E. coli. *Genes Dev.* **2017**, *31*, 1382−1395.

(29) Tsui, H. C.; Feng, G.; Winkler, M. E. Negative regulation of mutS and mutH repair gene expression by the Hfq and RpoS global regulators of *Escherichia coli* K-12. *J. Bacteriol.* **1997**, *179*, 7476−7487.

(30) Malabirade, A.; Partouche, D.; El Hamoui, O.; Turbant, F.; Geinguenaud, F.; Recouvreux, P.; Bizien, T.; Busi, F.; Wien, F.; Arluison, V. Revised role for Hfq bacterial regulator on DNA topology. *Sci. Rep.* **2018**, *8*, No. 16792.

(31) Malabirade, A.; Jiang, K.; Kubiak, K.; Diaz-Mendoza, A.; Liu, F.; van Kan, J. A.; Berret, J. F.; Arluison, V.; van der Maarel, J. R. C. Compaction and condensation of DNA mediated by the C-terminal domain of Hfq. *Nucleic Acids Res.* **2017**, *45*, 7299−7308.

(32) Zhang, A.; Altuvia, S.; Tiwari, A.; Argaman, L.; Hengge-Aronis, R.; Storz, G. The oxyS regulatory RNA represses rpoS translation and binds the Hfq (HF-1) protein. *EMBO J.* **1998**, *17*, 6061−6068.

(33) Møller, T.; Franch, T.; Hojrup, P.; Keene, D. R.; Bachinger, H. P.; Brennan, R. G.; Valentin-Hansen, P. Hfq. A Bacterial Sm-like Protein that Mediates RNA-RNA Interaction. *Mol. Cell* **2002**, *9*, 23−30.

(34) Azam, T. A.; Hiraga, S.; Ishihama, A. Two types of localization of the DNA-binding proteins within the *Escherichia coli* nucleoid. *Genes Cells* **2000**, *5*, 613−626.

(35) Azam, T. A.; Ishihama, A. Twelve species of the nucleoid-associated protein from *Escherichia coli*. Sequence recognition specificity and DNA binding affinity. *J. Biol. Chem.* **1999**, *274*, 33105−33113.

(36) Diestra, E.; Cayrol, B.; Arluison, V.; Risco, C. Cellular electron microscopy imaging reveals the localization of the Hfq protein close to the bacterial membrane. *PLoS One* **2009**, *4*, No. e8301.

(37) Wilusz, C. J.; Wilusz, J. Lsm proteins and Hfq: Life at the 3′ end. *RNA Biol.* **2013**, *10*, 592−601.

(38) Vogel, J.; Luisi, B. F. Hfq and its constellation of RNA. *Nat. Rev. Microbiol.* **2011**, *9*, 578−589.

(39) Orans, J.; Kovach, A. R.; Hoff, K. E.; Horstmann, N. M.; Brennan, R. G. Crystal structure of an *Escherichia coli* Hfq Core (residues 2-69)-DNA complex reveals multifunctional nucleic acid binding sites. *Nucleic acids Res.* **2020**, *48*, 3987−3997.

(40) Fortas, E.; Piccirilli, F.; Malabirade, A.; Militello, V.; Trepout, S.; Marco, S.; Taghbalout, A.; Arluison, V. New insight into the structure and function of Hfq C-terminus. *Biosci. Rep.* **2015**, *35*, No. e00190.

(41) Partouche, D.; Militello, V.; Gomesz-Zavaglia, A.; Wien, F.; Sandt, C.; Arluison, V. In situ characterization of Hfq bacterial amyloid: a Fourier-transform infrared spectroscopy study. *Pathogens* **2019**, *8*, 36.

(42) Hwang, W.; Arluison, V.; Hohng, W. Dynamic competition of DsrA and rpoS fragments for the proximal binding site of Hfq as a means for efficient annealing. *Nucleic Acids Res.* **2011**, *39*, 5131−5139.

(43) Geinguenaud, F.; Calandrini, V.; Teixeira, J.; Mayer, C.; Liquier, J.; Lavelle, C.; Arluison, V. Conformational transition of DNA bound to Hfq probed by infrared spectroscopy. *Phys. Chem. Chem. Phys.* **2011**, *13*, 1222−1229.

(44) Marrington, R.; Dafforn, T. R.; Halsall, D. J.; MacDonald, J. I.; Hicks, M.; Rodger, A. Validation of new microvolume Couette flow linear dichroism cells. *Analyst* **2005**, *130*, 1608−1616.

(45) Chevry, L.; Sampathkumar, N. K.; Cebers, A.; Berret, J. F. Magnetic wire-based sensors for the microrheology of complex fluids. *Phys. Rev. E: Stat., Nonlinear, Soft Matter Phys.* **2013**, *88*, No. 062306.

(46) Berret, J. F. Local viscoelasticity of living cells measured by rotational magnetic spectroscopy. *Nat. Commun.* **2016**, *7*, No. 10134.

(47) Loosli, F.; Najm, M.; Berret, J. F. Viscoelasticity of model surfactant solutions determined by magnetic rotation spectroscopy. *Colloids Surf., A* **2016**, *510*, 143−149.

(48) Yan, M.; Fresnais, J.; Sekar, S.; Chapel, J. P.; Berret, J. F. Magnetic nanowires generated via the waterborne desalting transition pathway. *ACS Appl. Mater. Interfaces* **2011**, *3*, 1049−1054.

(49) Colin, R.; Chevry, L.; Berret, J.-F.; Abou, B. Rotational microrheology of Maxwell fluids using micron-sized wires. *Soft Matter* **2014**, *10*, 1167−1173.

(50) Gu, Y.; Kornev, K. G. Ferromagnetic nanorods in applications to control of the in-plane anisotropy of composite films and for in situ characterization of the film rheology. *Adv. Funct. Mater.* **2016**, *26*, 3796−3808.

(51) Tokarev, A.; Yatvin, J.; Trotsenko, O.; Locklin, J.; Minko, S. Nanostructured Soft Matter with Magnetic Nanoparticles, Advanced Functional Materials. *Adv. Funct. Mater.* **2016**, *26*, 3761−3782.

(52) Thai, L. P. A.; Mousseau, F.; Oikonomou, E. K.; Berret, J. F. On the rheology of pulmonary surfactant: Effects of concentration and consequences for the surfactant replacement therapy. *Colloids Surf., B* **2019**, *178*, 337−345.

(53) Thai, L.-P.-A.; Mousseau, F.; Oikonomou, E.; Radiom, M.; Berret, J.-F. Effect of Nanoparticles on the Bulk Shear Viscosity of a Lung Surfactant Fluid. *ACS Nano* **2020**, *14*, 466−475.

(54) Refregiers, M.; Wien, F.; Ta, H. P.; Premvardhan, L.; Bac, S.; Jamme, F.; Rouam, V.; Lagarde, B.; Polack, F.; Giorgetta, J. L.; Ricaud, J. P.; Bordessoule, M.; Giuliani, A. DISCO synchrotron-radiation circular-dichroism endstation at SOLEIL. *J. Synchrotron Radiat.* **2012**, *19*, 831−835.

(55) Wien, F.; Wallace, B. A. Calcium fluoride micro cells for synchrotron radiation circular dichroism spectroscopy. *Appl. Spectrosc.* **2005**, *59*, 1109−1113.

(56) Lees, J. G.; Smith, B. R.; Wien, F.; Miles, A. J.; Wallace, B. A. CDtool-an integrated software package for circular dichroism spectroscopic data processing, analysis, and archiving. *Anal. Biochem.* **2004**, *332*, 285−289.

(57) Jackson, T. C.; Sukhodolets, M. V. Functional analyses of putative PalS (Palindromic Self-recognition) motifs in bacterial Hfq. *Biochem. Biophys. Res. Commun.* **2017**, *486*, 1048−1054.

(58) Jiang, K.; Zhang, C.; Guttula, D.; Liu, F.; van Kan, J. A.; Lavelle, C.; Kubiak, K.; Malabirade, A.; Lapp, A.; Arluison, V.; van der Maarel, J. R. Effects of Hfq on the conformation and compaction of DNA. *Nucleic Acids Res.* **2015**, *43*, 4332−4341.

(59) Frka-Petesic, B.; Erglis, K.; Berret, J.; Cebers, A.; Dupuis, V.; Fresnais, J.; Sandre, O.; Perzynski, T. Dynamics of Paramagnetic Nanostructured Rods under Rotating Field. *J. Magn. Magn. Mater.* **2011**, *323*, 1309−1313.

(60) Helgesen, G.; Pieranski, P.; Skjeltorp, A. Nonlinear phenomena in systems of magnetic holes. *Phys. Rev. Lett.* **1990**, *64*, 1425−1428.

(61) Larson, R. *The Structure and Rheology of Complex Fluids*; Oxford University Press: New York, 1998.

(62) Zhu, X.; Kundukad, B.; van der Maarel, J. R. Viscoelasticity of entangled λ-phage DNA solutions. *J. Chem. Phys.* **2008**, *129*, No. 185103.

(63) Mason, T. G. Estimating the viscoelastic moduli of complex fluids using the generalized Stokes−Einstein equation. *Rheol. Acta* **2000**, *39*, 371−4378.

(64) Schleif, R. DNA looping. *Annu. Rev. Biochem.* **1992**, *61*, 199−223.

(65) Raeside, C.; Gaffe, J.; Deatherage, D. E.; Tenaillon, O.; Briska, A. M.; Ptashkin, R. N.; Cruveiller, S.; Medigue, C.; Lenski, R. E.; Barrick, J. E.; Schneider, D. Large chromosomal rearrangements during a long-term evolution experiment with *Escherichia coli*. *mBio* **2014**, *5*, e01377−14.

(66) Chong, S.; Chen, C.; Ge, H.; Xie, X. S. Mechanism of transcriptional bursting in bacteria. *Cell* **2014**, *158*, 314−326.

(67) Sinden, R. R.; Pettijohn, D. E. Chromosomes in living *Escherichia coli* cells are segregated into domains of supercoiling. *Proc. Natl. Acad. Sci. U.S.A.* **1981**, *78*, 224−228.

(68) Sinden, R. R.; Carlson, J. O.; Pettijohn, D. E. Torsional tension in the DNA double helix measured with trimethylpsoralen in living *Escherichia coli* cells: analogous measurements in insect and human cells. *Cell* **1980**, *21*, 773−783.